PUBLICATION I

Josephson junction microwave amplifier in self-organized noise compression mode

Sci. Rep. 2, 276.

SCIENTIFIC REPORTS

OPEN

SUBJECT AREAS:
ELECTRONIC MATERIALS AND DEVICES
APPLIED PHYSICS
SUPERCONDUCTING MATERIALS
QUANTUM PHYSICS

Received
13 September 2011

Accepted
31 January 2012

Published
20 February 2012

Correspondence and requests for materials should be addressed to P.L. (pasi.lahteenmaki@ltl.tkk.fi) or P.H. (pertti.hakonen@aalto.fi)

*These authors contributed equally.

Josephson junction microwave amplifier in self-organized noise compression mode

Pasi Lähteenmäki[1]*, Visa Vesterinen[2]*, Juha Hassel[2], Heikki Seppä[2], & Pertti Hakonen[1]

[1]Low Temperature Laboratory, Aalto University, P.O.Box 15100, 00076 AALTO, Finland, [2]VTT Technical Research Centre of Finland, P.O. Box 1000, 02044 VTT, Finland.

The fundamental noise limit of a phase-preserving amplifier at frequency $\omega/2\pi$ is the standard quantum limit $T_q = \hbar\omega/2k_B$. In the microwave range, the best candidates have been amplifiers based on superconducting quantum interference devices (reaching the noise temperature $T_n \sim 1.8\mathrm{T_q}$ at 700 MHz), and non-degenerate parametric amplifiers (reaching noise levels close to the quantum limit $T_n \approx \mathrm{T_q}$ at 8 GHz). We introduce a new type of an amplifier based on the negative resistance of a selectively damped Josephson junction. Noise performance of our amplifier is limited by mixing of quantum noise from Josephson oscillation regime down to the signal frequency. Measurements yield nearly quantum-limited operation, $T_n = (3.2 \pm 1.0)\mathrm{T_q}$ at 2.8 GHz, owing to self-organization of the working point. Simulations describe the characteristics of our device well and indicate potential for wide bandwidth operation.

The goal of quantum limited amplification at microwave frequencies has become increasingly important for superconducting qubits and nanoelectromechanical systems[1]. The lowest noise temperatures with respect to the quantum noise have been achieved using nondegenerate parametric amplifiers based on superconducting quantum interference devices (SQUIDs)[2–4]. They yield a noise temperature T_n of about (1.0 – 1.6) $\mathrm{T_q}$. Other implementations of near-quantum limited amplification have been realized by means of Josephson ring oscillators[5], DC-SQUIDs[6,7], and parametric amplifiers based on Josephson junction arrays[2,8–11]. Devices based on photon-assisted tunneling SIS-mixers yield $T_n = 1.2\mathrm{T_q}$[12]. However, these devices lack power gain but they do have a large gain in photon number due to conversion from high to low frequency.

Negative differential resistance devices, in particular tunnel diodes, have been used in the past to construct oscillators and amplifiers for microwave frequencies. These devices are capable of very fast operation. They were among the first ones to be used at microwave frequencies because they display little or no excess noise in the negative resistance bias region[13]. Here, we propose a negative-resistance amplifier based on an unshunted, single Josephson junction (JJ) operating in a noise compression mode. Unshunted junctions have been analyzed and demonstrated to work in SQUID circuits at low frequencies by Seppä et al.[14]. We have developed analogous concepts for high frequency operation. The present device differs markedly from previous implementations using unshunted Josephson devices due to the modified impedance environment.

Unshunted junctions are attractive as low-noise devices since they minimize fluctuations by avoiding unnecessary dissipation in the junction environment. In voltage-biased (V_b) operation, these devices can be considered as mixers between the signal frequency (ω_s around a few GHz) and the Josephson frequency ($\omega_J = (2e/\hbar)\, V_\mathrm{b} = 2\pi \times 10 – 300$ GHz) including sidebands[15]. A frequency-dependent environmental impedance can be employed for controlling mixing strengths (because the Josephson junction is a phase driven current generator) and the impedance makes the conversion between these two quantities.

Results

The fundamental macroscopic principle of our single junction amplifier (SJA) is that the intrinsic resistance of a JJ is negative over time scales much longer than $1/\omega_J$[14] (as shown in Fig. 1a). This is usually hidden in weakly damped JJs since the negative-resistance branch is unstable. On the other hand, for strongly damped junctions, the total dynamic resistance is positive. This can be seen from the current-voltage IV characteristics $v_\mathrm{b} = \sqrt{i_b^2 - 1}$ for a Josephson junction with negligible capacitance (valid for $i_\mathrm{b} > 1$). Here $v_\mathrm{b} = V_\mathrm{b}/I_cR$ denotes the voltage scaled with critical current I_c and the shunt resistance R while $i_\mathrm{b} = I_\mathrm{b}/I_c$ is the dimensionless current. Solving for the current through the junction alone, $i_\mathrm{JJ} = i_\mathrm{b} - v_\mathrm{b}$ (illustrated by the black

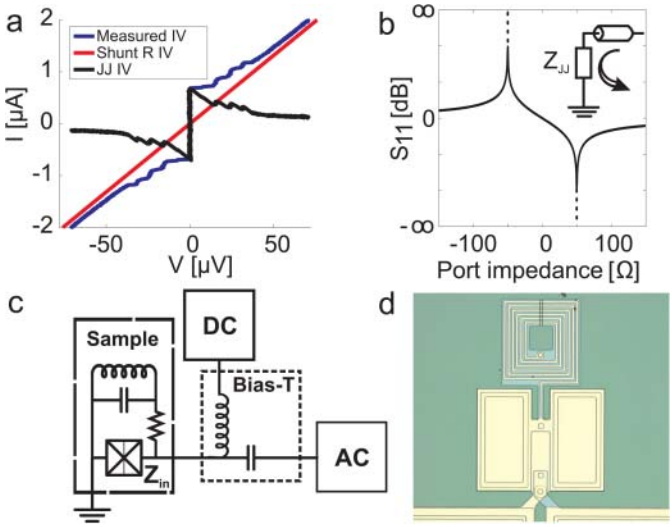

Figure 1 | a) Typical IV of a SJA (in blue); red and black curves indicate the division of I into shunt and junction currents, respectively. b) Reflection (scattering) amplitude S_{11} in a $Z_0 = 50\,\Omega$ system as a function of the load impedance. c) Principal scheme of the SJA operation. d) Optical image of a SJA; the size of the image is approximately 270 μm × 230 μm.

curve in Fig. 1a), we get for the scaled dynamic resistance

$$r_d = \frac{R_d}{R} = \frac{1}{di_{\rm JJ}/dv_{\rm b}} = \frac{1}{di_{\rm b}/dv_{\rm b} - 1} \qquad (1)$$

This yields $\sqrt{v_{\rm b}^2+1}/\left(v_{\rm b}-\sqrt{v_{\rm b}^2+1}\right)$, negative at all bias points.

The schematics of our SJA configuration is illustrated in Fig. 1c. To utilise the negative resistance of a JJ for amplification, stable operation has to be maintained by sufficient damping at all frequencies. The frequency-dependent damping is set in such a way that the external shunt damps the low ($\omega < \omega_s$, the signal frequency) and high ($\omega > \omega_s$) frequency dynamics, which ensures both stable DC bias and overdamped Josephson dynamics. In practice, we have realised this separation by mounting the shunt resistor in series with a bandstop filter whose center frequency is at the signal frequency ω_s[16,17]. The shunt capacitor is chosen large enough that it acts as a short at the Josephson frequency to ensure the high frequency dynamics and the IV curve are not modified. The stabilization in the stop band is provided by the postamplification circuit. The shunt circuit and the postamplification circuit together guarantee the stability of the device by generating a wide-band resistive environment for the JJ. Operated as a reflection amplifier, the power gain $|S_{11}(\omega)|^2 = |\Gamma(\omega)|^2$ is determined by the reflection coefficient

$$\Gamma(\omega) = (Z_{in}(\omega) - Z_0)/(Z_{in}(\omega) + Z_0), \qquad (2)$$

where $Z_{in}(\omega)$ is the impedance of the JJ, the shunt and the series inductance; Z_0 is the impedance of the readout circuit. As seen from the curve in Fig. 1b, there is gain ($S_{11} > 0$ dB) at all values of negative resistance and a strong divergence around $Z_{in} = -Z_0$. In the stopband of the shunt circuit, the input impedance $Z_{\rm in}(\omega_s)$ consists of the JJ (and possibly of an LC impedance transformer): it is real and negative. For $|R_d| \gtrsim Z_0$, large gain with stable operation can be obtained. For operating conditions where $|R_d| \gg Z_0$ impedance transforming circuits are employed to change the reference level impedance Z_0, *e.g.* from 50 Ω typical for standard RF technology to a level of 1 kΩ which is a typical value of $|R_d|$ for small Josephson junctions at high bias voltages.

The dynamics of SQUID circuits can be analyzed using a Langevin type of differential equation for the phase variable φ across the Josephson junctions[18]. Good agreement of such Langevin analysis with measured experimental results has been obtained in the past[19,20]. In the semiclassical approach, the generalized Nyquist noise formula by Callen and Welton[21] with the frequency dependence $0.5\hbar\omega$ coth $(\hbar\omega/2k_BT)$ is employed as the colored noise source in the differential equation[19,22,23]. At the Josephson frequency, the semiclassical noise power per unit bandwidth is so large ($\propto \hbar\omega_J \gg k_BT$) that, after downmixing, it will have observable effects on the phase dynamics at the signal frequency ω_s. Since the noise at ω_s is cut off from the Josephson junction by the bandstop filter (see Fig. 1c), direct noise from the shunt is avoided and only the down-mixed noise is present in our device. The absence of direct noise ensures good noise characteristics for our SJA and this feature is one of the basic differences when comparing SJAs with traditional microwave SQUID amplifiers.

Experimental. Fig. 2 displays noise spectra measured on the device at different bias points. At low bias currents, the magnitude of the dynamic resistance $|R_d|$ is smaller than the environmental impedance in parallel to it, making the total damping impedance of the LC resonator in the shunt circuit negative. This leads to either spontaneous oscillations or saturation. The oscillations are highly nonlinear, which is manifested as higher harmonics in the spectra. The saturation shows up as vanishing response. As $|R_d|$ increases at higher bias points, the system is stabilized and the harmonics disappear since the device operates as a linear amplifier generating amplified noise at the output.

After finding the optimal stable bias point, the gain vs. frequency was recorded at several power levels. The maximum measured gain of the SJA was found to be 28.3 ± 0.2 dB. The measured power gain of the device is plotted in Fig. 3 at $P_{\rm in} = -160$ dBm. The −1 dB compression point for $P_{\rm in}$ was found to be around −134 dBm; this yields a dynamic range of 70 dB as the input noise corresponds to −204 dBm. For the −3 dB bandwidth, we obtain BW ≃ 1 MHz. However, the bandwidth depends very much on the bias voltage due to the variation of R_d along the IV-curve, indicating that fundamentally the device is capable of wideband gain. In the present experiments, we reached $|\Gamma|_{\rm max} \times {\rm BW} = 40$ MHz for the voltage gain - bandwidth product. The nominal parameters of the measured amplifier are given in Table I in the Methods section.

The inset in Fig. 3 displays the improvement of the signal to noise ratio when the SJA is switched on and operated at its maximum gain. Based on this improvement, we find that the input-referred noise power added by the amplifier is 220 ± 70 mK ($0.5\hbar\omega/k_B$ coth$(\hbar\omega/2k_BT) = 90$ mK originating from the source has been subtracted), which corresponds to $T_n \approx (3.2 \pm 1.0)\, T_q$. The best noise temperature was obtained at the largest gain of the SJA.

Theoretical. To theoretically model a single junction device with arbitrary, frequency-dependent environment with $0 < \beta_c = 2eR^2(\omega)I_cC_J/\hbar < 1$, we simulate numerically the electrical circuit on the basis of the DC and AC Josephson relations which define a nonlinear circuit element having the properties: $I_{\rm J} = I_c \sin\varphi$ and $V = (\hbar/2e)\,\partial\varphi/\partial t$. We have compared our numerical simulations with analytic methods using an approximate model where we have adapted the resistively and capacitively shunted junction (RCSJ) approach to the modified environmental impedance of the SJA. Our numerical and analytic models take into account the Callen and Welton quantum noise from the environment semiclassically. Down-conversion of the noise at ω_J is the main quantity to be minimized for optimum performance.

The simulated power gain is included in Fig. 3 together with the experimental data. The theoretical gain curve is seen to follow the experimental behavior closely and it yields 42 MHz for the gain-bandwidth product. The simulated maximum gain amounts to 28.9 ± 0.5 dB. All these findings are in excellent agreement with the experimental data. Basically, the shape of the gain curve indicates that the amplification mechanism is based on mixing between ω_s and the sidebands of ω_J. This occurs along with the conversion from

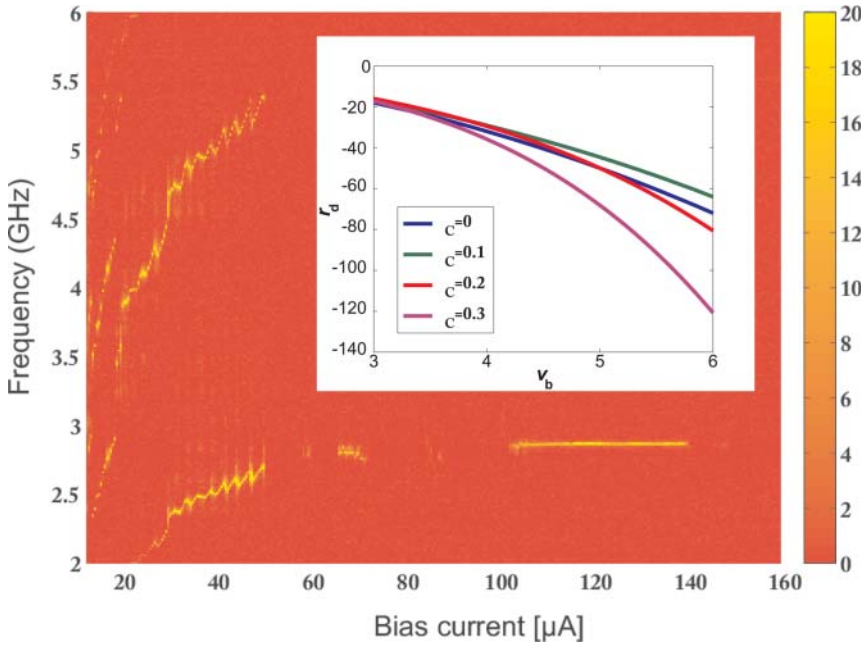

Figure 2 | Noise spectra of the device as function of the bias point; the reference level corresponds to 14 K k_B and the power scale on the right is given in dB. The inset displays the dependence of r_d as a function of bias voltage for different values of β_C. Values between 0 and r_d^* lead to unstable behaviour; $r_d^* = -50$ without impedance transformer ($R = 1\ \Omega$). There are no special features in the noise spectral density in the area below the inset.

down-mixed currents at ω_s to voltage by the shunt impedance (see the Supplementary material). For comparison, we have also calculated a linearized response curve where the Josephson junction has been replaced by a negative resistance of $R_d = -1370\ \Omega$ from Eq. (1).

Our numerical simulations yield $T_n = 270 \pm 30$ mK which is close to the experimentally found $T_n = 220 \pm 70$ mK. Hot-electron effects were taken into account by using the model of Ref. 24, on the basis of which we estimated the electronic temperature in the shunt to be $T_e \simeq 400$ mK instead of the base temperature 70 mK. The noise temperature is not very sensitive to hot electron effects when the shunt is fully blocked by the LC resonator at the center frequency. However, when going away from the center frequency, direct noise may leak out from the shunt reducing the useful band to "a noise-temperature-limited" range. The simulated noise power spectrum and the corresponding T_n as a function of frequency are presented in Fig. 4.

In our analytic modeling, we have generalized the semiclassical treatment of Ref. 19 to finite capacitance C_J and combined the mixing analysis with the current-voltage characteristics derived in Ref. 23. For the noise analysis, we define a noise process $\varphi_s(t)$, band-limited near the signal frequency. Another noise process $\varphi_j(t)$ with $\langle\varphi_j(t)^2\rangle \ll 1$ covers the Josephson frequency and one pair of sidebands ($\omega_J \pm \omega_s$). φ_j has a small variance because of the low impedance of the junction capacitor at high Josephson frequency. We expand $i_J = \sin\varphi(t) \approx \sin(\omega_J t + \varphi_s + \varphi_j)$ in order to describe the junction as a

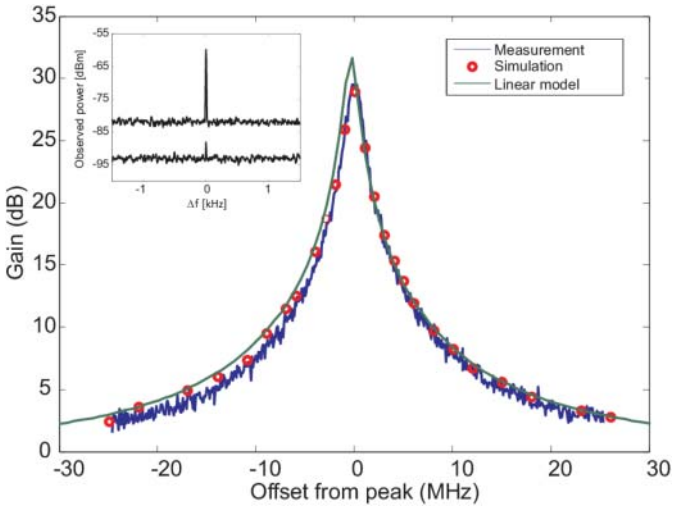

Figure 3 | Gain of the SJA as function of frequency at the optimal point of operation (blue, noisy curve). Results from our numerical simulation are denoted by open circles, while the smooth curve (green) illustrates the gain from a linearized electrical circuit model where the Josephson junction is replaced by a negative resistance of $R_d = -1370\ \Omega$ from Eq. (1). Inset: Output noise spectra having the SJA off (lower trace) and on (at maximum gain).

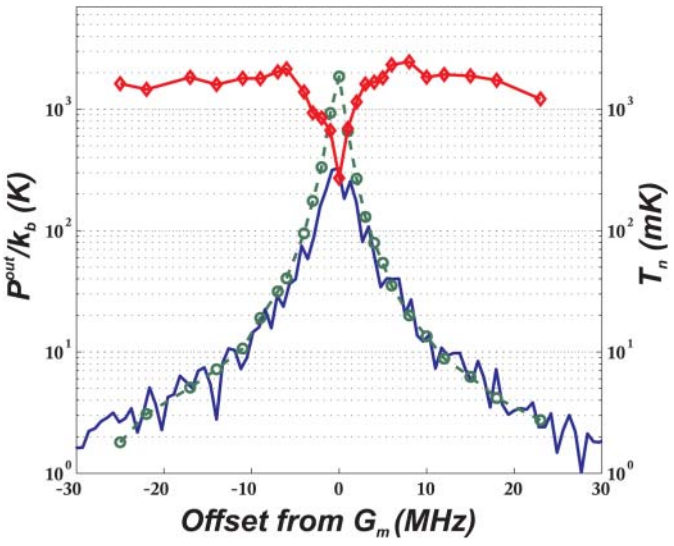

Figure 4 | The effective output noise temperature P_n^{out}/k_B (left scale) is compressed in the simulation (denoted by solid blue line) when compared with the product of the simulated gain (G – 1) and the uncompressed down-mixed noise of 2.4 K×k_b from Eq. 3 (○). After dividing the simulated output spectrum by the calculated gain, a clear dip is revealed in the input noise temperature (◇, right scale).

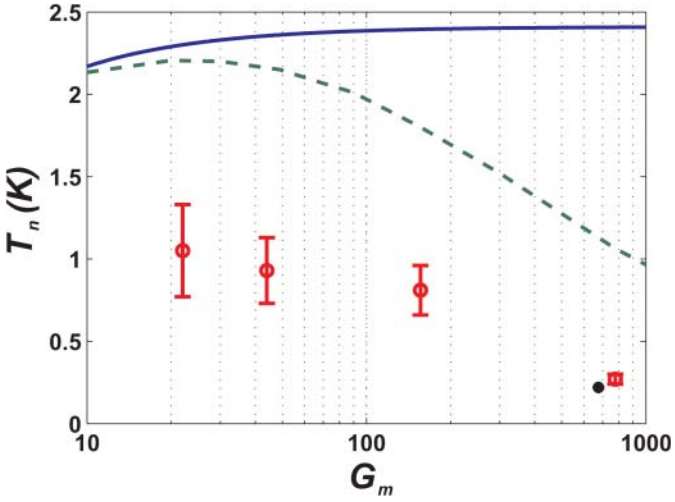

Figure 5 | Input noise temperature T_n vs. maximum gain of the SJA. The uncompressed T_n (Eq. (3) with $\xi = 1$, solid blue line) converges to 2.4 K at high gain. Compression suppressed T_n for the analytic model with two sidebands at $\omega_J \pm \omega_s$ is denoted by the dashed green line. Noise temperature from the simulations is depicted using open circles, and the error bars represent the statistical uncertainty in the simulated spectral density. The measurement result is marked by a filled circle (•), while the standard quantum limit would be $T_q = \hbar\omega/2k_B = 70$ mK.

DC current generator plus two AC current noise generators: one at ω_s and the other around the Josephson frequency. In the Fourier plane, the AC Josephson relation and the impedance environments at low and high frequencies establish the down-mixing noise process. We denote the variance of the phase noise over the signal band by $\delta_s^2 = \langle \phi_s(t)^2 \rangle$. In our calculations, we expand $\exp(i\varphi_s) \approx J_0(r) + i(2J_1(r)/r)\varphi_s$ (which is a good approximation at small δ_s^2) but this breaks down when additional sidebands ($\omega_J \pm 2\omega_s$ and so on) become significant. These Bessel functions of the first kind have the phase noise amplitude r divided by the signal band. Ideally, r should follow the Rayleigh distribution. In our analysis, we treat separately the limit of small fluctuations, $\delta_s^2 \ll 1$, and the regime with $\delta_s^2 \geq 1$, in which noise compression effects appear. With large gain and resonantly boosted current-voltage conversion, the phase fluctuations will grow so much that the non-linearities begin to limit the gain, and the system is driven to a steady state where the down-mixing process becomes altered and significantly suppressed. The number of added quanta per unit band from mixed-down noise is derived in the Supplementary material:

$$\frac{k_B T_{\mathrm{mix}}}{\hbar\omega_s} = \frac{N\xi(\delta_s^2)}{2}\left(\frac{1+\beta_c^2 v_b^2}{1+3\beta_c^2 v_b^2}\right)\left(\frac{G_m - 1}{Gm}\right), \qquad (3)$$

where $N = \omega_J/\omega_s$ and the factor $(G_m - 1)/G_m$ can be neglected at large gain. Noise suppression is denoted by the compression factor $\xi(\delta_s^2) \leq 1$ which equals unity at $\delta_s^2 \ll 1$ and decreases towards zero with growing variance. In our model with the sidebands $\omega_J \pm \omega_s$, we obtain $\xi(\delta_s^2) = \langle J_0^2(r) \rangle \sim exp(-\delta_s^2)$. Hence, large improvement in noise performance can be achieved compared to the linear where $\xi(\delta_s^2) = 1$.

The role of noise compression in the operation of the SJA is illustrated in Fig. 4. For reference, we plot the uncompressed noise from Eq. (3) multiplied by the simulated gain. The output noise temperature from the actual simulation differs from it (an indication of noise compression). The simulated spectrum is rounded near the gain peak, which creates a dip in the input noise temperature.

In Fig. 5, the input noise temperature at G_m is plotted as a function of the gain. Linear theories predict convergence towards $T_n = 2.4$ K at $G_m \gg 1$ (from Eq. (3) by taking $\xi = 1$). Above a threshold gain of $\sim$ 13 dB, noise suppression sets in. From our analytic model with two sidebands $\omega_J \pm \omega_s$, we obtain $\xi = \langle J_0^2(r) \rangle = 0.44$ for the compression factor at $G_m = 28$ dB and the noise temperature reduces to $T_n = 1.0$ K. Compared with numerical simulations, the analytic model yields nearly 3–4 times larger value for T_n.

Discussion

The compression mechanism for noise is crucial for the high bias operation of the SJA since otherwise T_n would grow directly proportional to v_b (N in Eq. (3)). The operation with noise compression can be viewed as self-organization of the system. Microscopic degrees of freedom give rise to a macroscopic order which can be parametrized to describe the behavior of the system. In our device, the macroscopic ordering is dictated by the integrated noise over the amplified bandwidth. This parameter governs the macroscopic characteristics of the device (e.g. the effective critical current and the gain of the device for external signals). The actual value of the gain is set by the higher order terms present in the Josephson energy, which resembles that of the order parameter stabilization in regular phase transitions.

The bandwidth of our SJA is fundamentally limited below the Josephson and plasma frequencies, $\frac{1}{2}\min(\omega_J, \omega_p)$. It can be shown that the gain-bandwidth product is $|\Gamma|_{\max} \times \mathrm{BW} = 2/|R_d|(C + C_J)$ in our first-order filtering scheme. In the measured amplifier, the capacitance of the bandstop filter is $C \approx 4.3$ pF and $C_J = 0.35$ pF. Furthermore, using $R_d = -1370\ \Omega$ as in our operating point of interest, the formula yields $|\Gamma|_{\max} \times \mathrm{BW} = 50$ MHz while $\approx$ 40 MHz is obtained experimentally. In general, stability of the amplifier requires that $C > C_J$. Reduction of the shunt capacitance facilitates improvement of the gainbandwidth product but the boundary condition $R \gg (\omega_J C)^{-1}$ must be met. High bandwidth is predicted at small R_d too, which can be obtained most effectively by increasing the critical current. Also C_J controls the value of R_d so that the optimum for gain-bandwidth product is obtained for a small junction with a high critical current density.

Another possible low noise regime for the SJA is the limit of small ω_J. We analyzed a few devices at $v_b = 3$ ($N = 2.33$) with different β_c (see the Suppl.). We obtained analytically that the down-mixed noise contribution is around $\hbar\omega$ at $\beta_c = 0.3 - 0.5$ without any noise

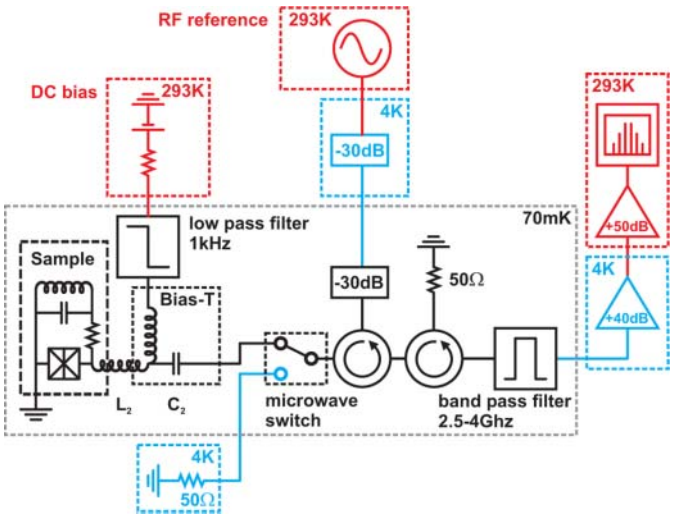

Figure 6 | Setup for measuring the SJA characteristics. The essential components of the SJA are located at 70 mK (indicated by the dashed black box). 60 dB of attenuation is employed to thermalize the incoming rf signal cable and two circulators eliminate the back action noise from the preamplifier. Noise temperature of the cooled preamplifier (including losses in front of the preamplifier) $T_n^{\mathrm{HEMT}} = 14 \pm 3$ K at the center frequency of the SJA.

Table I | SJA parameters in the experiment and the simulation. Definitions: Z_0, impedance of the source and the readout circuit; R, C and L the shunt resistance, capacitance and inductance, respectively; I_c, C_J, ω_p and β_c the critical current, the capacitance, plasma frequency and the Stewart-McCumber parameter of the junction, respectively; C_2, L_2 the capacitance and the inductance in series with the SJA device (impedance transformer); ω_s the signal frequency; I_b and ω_J the bias current and the Josephson frequency at the optimal operating point

Parameter	Value	Parameter	Value
Z_0	50 Ω	I_c	17 μA
R	4.0 Ω	C_J	0.35 pF
C	4.26 pF	$\omega_p/(2\pi)$	61 GHz
L	702 pH	β_c	0.29
C_2	33 pF	I_b	140 μA
L_2	14.25 nH	$\omega_J/(2\pi)$	270 GHz
ω_s	2.865 GHz		

compression. This was verified in numerical simulations according to which 0.9 ± 0.2 quanta were added by our SJA. Addition of one quantum indicates that the noise behaviour of the SJA is reminiscent to that of heterodyne detection where the image frequency brings an extra noise of $\frac{1}{2}\hbar\omega$ to the detected signal[25], i.e. both sidebands of the Josephson frequency add $\frac{1}{2}\hbar\omega$ to the noise temperature.

The control of noise in our SJA is not fully optimized and several issues should be addressed in order to make the theoretical procedure for noise minimization more effective and transparent. Using numerical simulations, we reproduced the measured noise temperature $3.2T_q$ at high bias and found signs for the complex behavior of our device. Our analytical model mixes down noise only from two sidebands $\omega_J \pm \omega_s$, the consideration of which is sufficient at low Josephson frequency and small phase noise variance δ_s^2. Consequently, the predictions of $T_n \sim \hbar\omega$ from our analytical modeling are reliable at low bias voltage. In the noise compression mode, $\delta_s^2 \geq 1$, our simulations show that the analytic model fails and an extension in the number of tracked sidebands is necessary. Moreover, further work will be needed to show whether pronounced noise compression can drive the SJA into the standard quantum limit T_q. Our analysis indicates that the concept of selectively shunted junction amplifier for microwaves is sound and that it provides the best route for quantum limited operation over large bandwidths.

Methods

Our experimental setup for the SJA measurements is shown in Fig. 6. The device is biased with a DC current which allows the effective value of the negative resistance to be tuned over a wide range of values. The incoming signal and the reflected signal are separated by circulators and the signal postamplification is performed by high electron mobility transistor (HEMT) based amplifiers at 4 K and at the room temperature. At the optimal operating point, the dynamic resistance R_d of the Josephson junction is $-1370\ \Omega$ in our amplifier. To get substantial gain according to Eq. 2, we apply impedance transformation by placing an inductor L_2 in series with the junction. This converts the input impedance $Z_{in}(\omega_s)$ close to $-50\ \Omega$.

To measure the amplifier performance, we injected a reference signal and recorded the signal-to-noise (S/N) ratio while having the SJA ON and OFF. In the OFF state, the SJA acts like a pure inductance reflecting all the incoming power (passive mirror) and the noise in the S/N ratio measurement is fully specified by the HEMT preamplifier. The largest improvement in the S/N was found at the highest bias current $\sim 140\ \mu$A ($i_b = 8.2$). Using a source at 70 mK, the S/N ratio after the HEMT amplifier was improved by 17.2 ± 0.2 dB. Thanks to the microwave switch in the setup, the noise temperature of the HEMT amplifier could be carefully calibrated using the cold/hot load technique. The parameters of the investigated amplifier are collected into Table I.

1. Clerk, A. A., Devoret, M. H., Girvin, S. M., Marquardt, F. & Schoelkopf, R. J. Introduction to quantum noise, measurement, and amplification. *Rev. Mod. Phys.* **81**, 1155–1208 (2010).
2. Hatridge, M., Vijay, R., Slichter, D. H., Clarke, J. & Siddiqi, I. Dispersive magnetometry with a quantum limited SQUID parametric amplifier. *Phys. Rev. B* **83**, 134501 (2011).
3. Yurke, B., Corruccini, L. R., Kaminsky, P. G. & Rupp, L. W. Observation of parametric amplification and deamplification in a Josephson parametric amplifier. *Phys. Rev. A*, **39**, 2519–2533 (1989).
4. Yurke, B. *et al.* A low-noise series-array Josephson junction parametric amplifier. *Appl. Phys. Lett.* **69**, 3078–3080 (1996)
5. Bergeal, N. *et al.* Phase-preserving amplification near the quantum limit with a Josephson ring modulator. *Nature* **465**, 64–68 (2010).
6. Mück, M., Kycia, J. B. & Clarke, J. Superconducting quantum interference device as a near-quantum-limited amplifier at 0.5 GHz. *Appl. Phys. Lett.* **78**, 967–969 (2001).
7. Asztalos, S. J. *et al.* SQUID-based microwave cavity search for dark-matter axions. *Phys. Rev. Lett.* **104**, 041301 (2010).
8. Castellanos-Beltran, M. A., Irwin, K. D., Hilton, G. C., Vale, L. R. & Lehnert, K. W. Amplification and squeezing of quantum noise with a tunable Josephson metamaterial. *Nature Physics* **4**, 929–931 (2008).
9. Teufel, J. D., Donner, T., Castellanos-Beltran, M. A., Harlow, J. W. & Lehnert, K. W. Nanomechanical motion measured with precision beyond the standard quantum limit. *Nature Nanotech.* **4**, 820–823 (2009).
10. Castellanos-Beltran, M. A. & Lehnert, K. W. A widely tunable parametric amplifier based on a SQUID array resonator. *Appl. Phys. Lett.* **91**, 083509 (2007).
11. Spietz, L., Irwin, K., Aumentado, K. & Aumentado, J. Input impedance and gain of a gigaherz amplifier using a dc superconducting quantum interference device in a quarter wave resonator. *Appl. Phys. Lett.* **93**, 082506 (2008).
12. Mears, C. A., *et al.* Quantum-limited heterodyne detection of millimeter waves using superconducting tantalum tunnel junctions. *Appl. Phys. Lett.* **57**, 2487–2489 (1990).
13. Tiemann, J. J. Shot noise in tunnel diode amplifiers. *Proc. IRE.* **8**, 1418–1423 (1960).
14. Seppä, H., Kiviranta, M., Grönberg, L. DC SQUID based on unshunted Josephson junctions: Experimental results. *IEEE Trans. Appl. Supercond.* **5**, 3248–3251 (1995).
15. Likharev, K. K. *Dynamics of Josephson junctions and circuits* (Gordon and Breach, New York, 1986).
16. Vystavkin, A., *et al.* One- frequency parametric amplifier using self-pumped Josephson junction. *Magnetics, IEEE Trans.* **13**, 233–236 (1977).
17. Calander, N., Claeson, T. & Runder, S. Shunted Josephson tunnel junctions: High-frequency, self-pumped low noise amplifiers. *J. Appl. Phys.*, **53**, 5093–5103 (1982).
18. Clarke, J. & Braginsky, A. I. eds., *The SQUID Handbook*, volume 1 (Wiley, Weinheim, 2004).
19. Koch, R. H., Van Harlingen, D. J. & Clarke, J. Measurements of quantum noise in resistively shunted Josephson junctions. *Phys. Rev. B*, **26**, 74 (1982).
20. Likharev, K. K. & Semenov, V. K. Fluctuation spectrum in superconducting point contacts. *Zh. Eksp. Teor. Fiz. Pis'ma* **15**, 625 (1972) JETP Lett. **15**, 442 (1972).
21. Callen, H. B. & Welton, T. A. Irreversibility and generalized noise. *Phys. Rev.* **83**, 34–40 (1951).
22. Levinson, Y., Quantum noise in a current-biased Josephson junction. *Phys. Rev. B* **67**, 184504 (2003).
23. Brandt, F. T. Frenkel, J. & Taylor, J. C. Noise in resistively shunted Josephson junctions. *Phys. Rev. B* **82**, 014515 (2010).
24. Wellstood, F. C. Urbina, C. & Clarke, J. Hot-electron effects in metals. *Phys. Rev. B* 49, 5942–5955 (1994).
25. Haus, H. A. *Electromagnetic noise and quantum optical measurements*, Ch. 8, (Springer, Berlin, 2000).

Acknowledgements

We thank Jari Penttilä for providing the Josephson junctions used in our experiments. We also thank Thomas Aref for his support during the writing of this article. This work was supported by Center of Excellence and Materials World Network grants of the Academy of Finland and by the European Science Foundation (ESF) under the EUROCORES Programme EuroGRAPHENE.

Author contributions

All authors took jointly part in the planning of this experimental work and the development of its theoretical interpretation. P. L. performed the experiments and V. V. made the numerical simulations and the analytical mixing analysis. P. L. and V. V. co-operatively wrote the first versions of the main manuscript and the Supplementary material. All authors contributed to editing of the manuscript.

Additional information

Supplementary information accompanies this paper at http://www.nature.com/scientificreports

Competing financial interests: The authors declare no competing financial interests.

How to cite this article: Lähteenmäki, P. *et al.* Josephson junction microwave amplifier in self-organized noise compression mode. *Sci. Rep.* **2**, 276; DOI:10.1038/srep00276 (2012).

Josephson junction microwave amplifier in the noise compression mode: Supplementary material

Pasi Lähteenmäki*†,[1] Visa Vesterinen†,[2] Juha Hassel,[2] Heikki Seppä,[2] and Pertti Hakonen[1]

[1] *Low Temperature Laboratory, Aalto University, P.O.Box 15100, 00076 AALTO, Finland*

[2] *VTT Technical Research Centre of Finland, P.O. Box 1000, 02044 VTT, Finland*

[†]These authors contributed equally.

CONTENTS

Our Supplementary material is divided into chapters as outlined above. Ch. I details the circuit diagram of the single junction amplifier (SJA). The non-linear Josephson junction element and the semiclassical, quantum noise generators are defined, and we derive the Langevin system of differential equations that is solved numerically in the time domain. In Ch. II, we study the amplifier characteristics analytically by introducing a linear model where the Josephson junction is replaced by negative dynamic resistance R_d. In particular, the magnitude of R_d is linked to DC voltage bias and junction capacitance. Equations for down-mixed noise from the Josephson frequency are derived and analyzed in detail. Ch. III deals with guidelines for practical amplifier design and summarizes the constraints that limit the

parameter selection. Relations between gain, bandwidth, and stability are studied. Finally, Ch. IV presents the results. At high-bias operation point, the experiment is compared with the simulations of Ch. I and the analytic model of Ch. II. We also present numerical results of a nearly quantum limited amplifier at low bias, designed using principles given in Ch. III.

I. COMPUTATIONAL METHODS

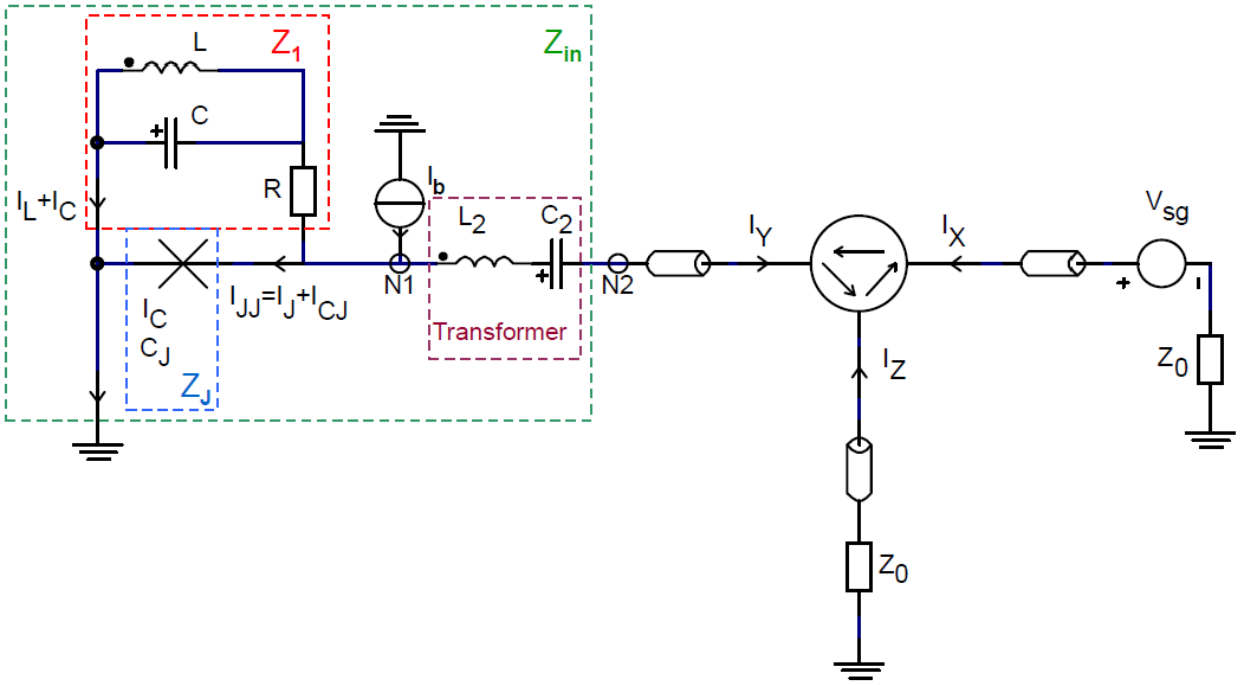

FIG. 1. Amplifier circuit with a Josephson junction denoted by the cross. Node N1 specifies the node to which the bias current I_b is fed. A circulator connects the branches X, Y, and Z in a manner denoted by the arrows; the amplifier input impedance Z_in is the impedance at $N2$ looking outward from port Y. The junction has internal capacitance C_J which is not drawn explicitly. For the variables, see text.

The circuit diagram of the analyzed SJA Josephson amplifier is presented in Fig. 1. Using the standard definitions for the Josephson current I_J and the voltage V

$$I_\mathrm{J} = I_\mathrm{c} \sin\varphi \tag{1}$$

$$V = \frac{\hbar}{2e}\frac{\partial\varphi}{\partial t} = \frac{\Phi_0}{2\pi}\frac{\partial\varphi}{\partial t}, \tag{2}$$

we can model the non-linear behavior of the junction in an otherwise regular electrical circuit.

The critical current I_c and the phase difference φ are measured across the junction. The constants e and $\hbar$ denote the elementary charge and reduced Planck's constant, respectively; $\Phi_0 = \pi\hbar/e$ is the flux quantum. Other quantities in Fig. 1 are understood through

- C_J, I_CJ: junction capacitance and current flowing through it
- R, $I_R + \delta I$: resistance of the bandstop shunt and the current in it with fluctuation δI
- L, I_L, C, I_C: shunt inductor, capacitor, and the associated currents
- I_b, V_sg: current bias and signal voltage generators
- L_2, C_2: LC transformer for impedance matching
- I_X, $I_\mathrm{Y} \equiv -I_2$, I_Z: currents entering the three-port circulator (they sum up to zero)
- Z_0: internal resistance of signal generator in branch X; matched load in branch Z.

Transformation into dimensionless variables written in lower case letters is defined as

$$\omega_\mathrm{p} = \sqrt{2\pi I_\mathrm{c}/(\Phi_0 C_\mathrm{J})} \text{ (plasma frequency)} \tag{3}$$

$$Q = \omega_\mathrm{p} R C_\mathrm{J} \text{ (quality factor)} \tag{4}$$

$$\tau = \omega_\mathrm{p} t \tag{5}$$

$$i_\mathrm{J} = I_\mathrm{J}/I_\mathrm{c} = \sin\varphi \tag{6}$$

$$v = V/(RI_\mathrm{c}) = \frac{1}{Q}\frac{\partial\varphi}{\partial\tau} = \frac{\varphi'}{Q}. \tag{7}$$

Similarly, all currents are divided by I_c, and voltages by the product RI_c. The dynamics of the Josephson junction in the presence of finite $C_J > 0$ is often described using the dimensionless Stewart-McCumber parameter $\beta_C = Q^2 = 2eR^2 I_c C_J/\hbar$. Charges in capacitors become dimensionless when they are multiplied by $\omega_\mathrm{p}/I_\mathrm{c}$. Dimensionless resistances r are multiples of R.

Kirchhoff's current law tells that

$$i_C + i_L = i_R + \delta i \text{ (in the shunt)} \tag{8}$$

$$i_2 + i = i_C + i_L + i_\mathrm{J} + i_\mathrm{CJ} \text{ (at node N1)} \tag{9}$$

$$i_\mathrm{X} + i_\mathrm{Z} = i_2 \equiv -i_\mathrm{Y} \text{ (at the circulator)}. \tag{10}$$

Electric power must be conserved within the circulator. Using an ideal circulator, we obtain for the voltages and currents at the three ports:

$$v_{\mathrm{X}} = \frac{v_{\mathrm{sg}}}{2} \;\&\; i_{\mathrm{X}} = \frac{R v_{\mathrm{sg}}}{2 Z_0} \tag{11}$$

$$v_{\mathrm{Y}} = v_{\mathrm{sg}} - \frac{Z_0 i_2}{R} \;(i_2 \text{ is a variable}) \tag{12}$$

$$v_{\mathrm{Z}} = \frac{v_{\mathrm{sg}}}{2} - \frac{Z_0 i_2}{R} \;\&\; i_{\mathrm{Z}} = -\frac{R v_{\mathrm{Z}}}{Z_0}. \tag{13}$$

Kirchhoff's voltage law yields

$$v = v_{\mathrm{sg}} - \frac{Z_0 i_2}{R} - \frac{L_2 \omega_{\mathrm{p}} i_2'}{R} - \frac{q_2}{\omega_{\mathrm{p}} R C_2} \tag{14}$$

(between nodes N1 and N2)

$$\frac{q}{\omega_{\mathrm{p}} R C} = \frac{L \omega_{\mathrm{p}} i_L'}{R} = v - i_R \tag{15}$$

(in the shunt),

where the primes denote time derivatives. The charges stored in the capacitors C and C_2 are related to the currents via $q' = i_C$ and $q_2' = i_2$, respectively. In the Josephson junction $q_{\mathrm{J}}' = i_{\mathrm{CJ}}$. We can gather all the information presented so far into a Langevin system of ordinary differential equations

$$\begin{pmatrix} \varphi' \\ q_{\mathrm{J}}' \\ q' \\ i_L' \\ q_2' \\ i_2' \end{pmatrix} = A \begin{pmatrix} \varphi \\ q_{\mathrm{J}} \\ q \\ i_L \\ q_2 \\ i_2 \end{pmatrix} + \begin{pmatrix} 0 \\ i_{\mathrm{b}} - \delta i - \sin\varphi \\ \delta i \\ 0 \\ 0 \\ \frac{R v_{\mathrm{sg}}}{L_2 \omega_{\mathrm{p}}} \end{pmatrix} \tag{16}$$

where matrix A is

$$\begin{pmatrix} 0 & 1 & 0 & 0 & 0 & 0 \\ 0 & -\frac{1}{Q} & \frac{C_{\mathrm{J}}}{CQ} & 0 & 0 & 1 \\ 0 & \frac{1}{Q} & -\frac{C_{\mathrm{J}}}{CQ} & -1 & 0 & 0 \\ 0 & 0 & \frac{\omega_0^2}{\omega_{\mathrm{p}}^2} & 0 & 0 & 0 \\ 0 & 0 & 0 & 0 & 0 & 1 \\ 0 & -\frac{C_2 \omega_2^2}{C_{\mathrm{J}} \omega_{\mathrm{p}}^2} & 0 & 0 & -\frac{\omega_2^2}{\omega_{\mathrm{p}}^2} & -\frac{Z_0}{L_2 \omega_{\mathrm{p}}} \end{pmatrix}. \tag{17}$$

Eigenfrequencies are $\omega_0 = 1/\sqrt{LC}$ and $\omega_2 = 1/\sqrt{L_2 C_2}$.

Josephson frequency $\omega_{\rm J} = 2eV_b/\hbar$, expressed through averaged Josephson voltage $V_b = \langle V \rangle$, is the quantity that determines the necessary bandwidth in the simulations. Two harmonics of $\omega_{\rm J}$ fit inside $3\omega_J$, and the interval of digitally filtered noise samples is set to $6\omega_J$ because of Nyquist sampling theorem. For the shunt resistor, we included symmetrized quantum noise which has current spectral density

$$S_I(\omega) = \frac{2\hbar\omega}{R} \coth\left(\frac{\hbar\omega}{2k_B T_{\rm shunt}}\right), \tag{18}$$

defined here as the variance of current per unit bandwidth at positive frequencies; k_B is Boltzmann's constant. The input noise, added to $v_{\rm sg}$, had the voltage spectral density ($\omega > 0$)

$$S_V(\omega) = 2Z_0\hbar\omega \coth\left(\frac{\hbar\omega}{2k_B T_{\rm in}}\right) \tag{19}$$

which corresponds to voltage variance per unit bandwidth. Input noise at temperature $T_{\rm in} = 70$ mK was bandpass filtered to take the circulator bandwidth into account. It can be noticed that half a quantum of noise of $\hbar\omega/2$ enters the amplifier input even at zero temperature (consider the product $v_{\rm X} i_{\rm X}$ in Eq. (11)).

Simulation was started by setting voltages, charges and currents to zero. First, the bias current $i_{\rm b}$ was slowly turned on and swept linearly up to a point where stability could be observed. The bias was then swept down to the desired operation point ($i_{\rm b} > 1$). Second, the amplifier was perturbed with a Gaussian input pulse from $v_{\rm sg}$ in order to confirm the stability. Finally, a sinusoidal input voltage was turned on, in the case when the reflection coefficient Γ of the system was to be evaluated. The coefficient gives the relation between input and output voltages: $v_{\rm Z}(\omega) = \Gamma(\omega) v_{\rm X}(\omega)$. The input impedance $Z_{\rm in}$ of the amplifier, or the impedance looking out from port Y, is easily obtained from

$$v_{\rm sg} = \frac{Z_{\rm in} + Z_0}{R} i_2. \tag{20}$$

The desired Fourier components of $v_{\rm sg}$ and i_2 are computed with FFT analysis on steady-state time traces. It turns out that

$$\Gamma(\omega) = \frac{Z_{\rm in} - Z_0}{Z_{\rm in} + Z_0} \tag{21}$$

as in regular microwave reflection measurements. Power gain of the amplifier can be estimated with $G = |\Gamma(\omega)|^2$, the squared modulus of the reflection coefficient. For more accurate

results, the spectral density of the output voltage v_{Z} is plotted in two distinct cases: (I) normal operation and (II) silent, unbiased situation with unity gain ($i_{\mathrm{b}} = i_2 = 0$). Input noise is present on top of the sinusoidal signal in v_{sg}, see Eq. (13). The gain is computed as the ratio of spectral densities in the cases (I) and (II) at the input frequency.

Noise added by the Josephson amplifier was estimated after the gain peak $G(\omega)$ had been found. Nothing but quantum noise was present at input v_{sg} during this simulation. The spectral density of v_{Z} was scaled by $(RI_{\mathrm{c}})^2/(k_B Z_0)$ to get total noise power referred to the output. The noise added by the amplifier, as referred to the input, could be obtained by dividing the result by G and subtracting the contribution of v_{sg}. The equivalent noise power of fluctuations entering the amplifier was calculated as the product of $(RI_{\mathrm{c}})^2/(4k_B Z_0)$ and the spectral density of v_{sg}. The subtracted amount equals

$$\frac{\hbar\omega}{2k_B} \coth\left(\frac{\hbar\omega}{2k_B T_{\mathrm{in}}}\right) \approx \ 90 \text{ mK}. \tag{22}$$

The intrinsic impedance of the Josephson junction, Z_{J}, could be estimated with steady-state FFT analysis of voltage v and total current $i_{\mathrm{J}} + i_{\mathrm{CJ}}$. We denote the dynamic resistance with R_{d} in equation

$$\frac{1}{Z_{\mathrm{J}}} = i\omega C_{\mathrm{J}} + \frac{1}{R_{\mathrm{d}}} \tag{23}$$

which can be manipulated to obtain

$$R_{\mathrm{d}} = -\frac{1}{\omega C_{\mathrm{J}}} \cdot \frac{\mathbb{I}\{Z_{\mathrm{J}}\}}{\mathbb{R}\{Z_{\mathrm{J}}\}} = -\frac{\tan\phi_{\mathrm{J}}}{\omega C_{\mathrm{J}}}. \tag{24}$$

The phase difference between v and $i_{\mathrm{J}} + i_{\mathrm{CJ}}$ equals ϕ_{J}.

II. ANALYTICAL METHODS

A. Direct noise

The direct noise is defined as the noise generated at the shunt resistor R in the signal band. It is described by the current generator δi in parallel with R. We derived the linear transfer function from fluctuating resistor voltage $\delta v_R = \delta i$ to output voltage v_Z. The transfer function has the shunt impedance Z_1 in the denominator, see Figure 1. Exactly at the shunt eigenfrequency, $\omega_0 = 1/\sqrt{LC}$, the direct noise becomes negligible as $|Z_1| \to \infty$. After a small offset from ω_0, the magnitude of the shunt reactance X_1 is finite but much

larger than R in the following equation:

$$Z_1 = R + (1/(i\omega L) + i\omega C)^{-1} = R + iX_1. \tag{25}$$

We may thus approximate

$$\frac{1}{Z_1} = \frac{R}{X_1^2} - \frac{i}{X_1},\ \omega \approx \omega_0, \tag{26}$$

and we obtain for the input-referred noise temperature

$$k_B T_{\text{direct}} = \frac{R|R_d|\hbar\omega}{2X_1^2} \coth\left(\frac{\hbar\omega}{2k_B T_{\text{shunt}}}\right),\ R^2 \ll X_1^2$$
$$X_1 = \frac{\omega L}{1-\omega^2 LC}. \tag{27}$$

B. Down-mixed noise

Here we present an analytic treatment for the noise generated in the shunt resistor at frequencies near the Josephson frequency and mixed down to signal frequency by Josephson dynamics. We divide the fluctuating phase over the Josephson junction $\varphi(t)$ into the three parts. First, φ_s is the noise close to the signal frequencies at the bandwidth determined by the frequency response of the environment, i.e., $Z_E(\omega)$. Second, φ_j describes the noise in the sidebands of the Josephson oscillation. Around the Josephson frequency, quantum noise φ_n is generated by the shunt resistance R which is the main source of dissipation there. In addition, the average phase varies as $\langle\varphi(t)\rangle = \omega_J t$ due to the voltage-driven Josephson oscillation at the high bias limit. The total phase can be written as

$$\varphi(t) = \omega_J t + \varphi_s(t) + \varphi_j(t) + \varphi_n(t). \tag{28}$$

Functions φ_s, φ_j are effectively band-limited due to the frequency-dependent environment. The simplest way to describe the noise spectra with narrow band is to use the envelope and phase representation [7], which leads to sinusoidal time dependence with a fluctuating amplitude and phase. For instance,

$$\varphi_s = r(t)\sin(\omega_s t + \psi(t)). \tag{29}$$

Using the sum rule of trigonometric functions, one can see that the random phase $\psi(t)$ only moves signal from one quadrature to the other, and this does not have any relevance for the

splitting of power between different frequencies. The spread of $r(t)$ is described by Rayleigh distribution which has the probability density function

$$f_R(r) = \frac{r}{\delta_s^2} e^{-r^2/(2\delta_s^2)} \tag{30}$$

where the variance of φ_s, or average power, is δ_s^2. Thus, we have reduced the problem of band limited noise to sinusoidal behavior with an approximately defined amplitude.

The impedance $Z_E(\omega)$ seen by the signal frequency current fluctuation is given in our case by

$$Z_E(\omega) = \frac{R_d Z_0'(\omega)}{R_d + Z_0'(\omega)} \tag{31}$$

where $Z_0'(\omega)$ is the impedance in parallel to the junction (in our circuit Z_0 transformed close to $|R_d|$ by the series L_2C_2 transformer). The resistance R of the bandstop filter is not visible in the signal band. Using $Z_E(\omega_s)$ for the conversion between current and voltage fluctuations at the signal frequency, we can easily calculate the input-referred noise temperature $k_B T_{mix} = Z_E^2 I_c^2 S_I(\omega_s)/(GZ_0')$, where the power gain $G = |(R_d - Z_0')/(R_d + Z_0')|^2$ is responsible for the reduction to the input. We will move into the Fourier plane to obtain the dimensionless noise current generator $S_I(\omega_s)$ in parallel to the junction. The phase fluctuation φ_j in the Josephson band is assumed to be small: $\langle \varphi_j^2 \rangle \ll 1$. We expand the Josephson current $\sin\varphi(t)$ (total phase is in Eq. (28)) and set $\cos\varphi_j \approx 1$, $\sin\varphi_j \approx \varphi_j$. The currents at high frequencies and at the signal frequency become

$$i_j(t) = \cos(\omega_J t)\sin\varphi_s + \sin(\omega_J t)\cos\varphi_s \tag{32}$$

$$i_s(t) = \varphi_j \cos(\omega_J t)\cos\varphi_s - \varphi_j \sin(\omega_J t)\sin\varphi_s, \tag{33}$$

respectively. The phase-to-current relation in the Josephson band reads

$$\hbar\dot{\varphi}_j = 2eV_J \tag{34}$$

$$-I_c i_j(\omega_J) = C_J \dot{V}_J + V_J/R, \tag{35}$$

in which V_J is the high-frequency part of Josephson voltage V. The current generators in parallel to the junction are $-i_s$ and $-i_j$. We adopt the Fourier transform convention $\hat{f}(\omega) = \int f(x) e^{-i\omega x} dx$. Since the Fourier transform of a product is a convolution, we obtain

the transforms

$$\hat{i}_j = \frac{1}{2}\left(\widehat{\sin\varphi_s}(\omega-\omega_J) - i\widehat{\cos\varphi_s}(\omega-\omega_J) + \widehat{\sin\varphi_s}(\omega+\omega_J) + i\widehat{\cos\varphi_s}(\omega-\omega_J)\right)$$
$$= \frac{i}{2}\left(-\widehat{e^{i\varphi_s}}(\omega-\omega_J) + \widehat{e^{-i\varphi_s}}(\omega+\omega_J)\right) \quad (36)$$

$$\hat{i}_s = \frac{1}{2}\left(\varphi_j\widehat{\cos\varphi}_s(\omega-\omega_J) + i\varphi_j\widehat{\sin\varphi}_s(\omega-\omega_J) + \varphi_j\widehat{\cos\varphi}_s(\omega+\omega_J) - i\varphi_j\widehat{\sin\varphi}_s(\omega+\omega_J)\right)$$
$$= \frac{1}{2}\left(\widehat{\varphi_j e^{i\varphi_s}}(\omega-\omega_J) + \widehat{\varphi_j e^{-i\varphi_s}}(\omega+\omega_J)\right). \quad (37)$$

Eqs. (34) and (35) now yield for the signal and Josephson bands

$$i\hbar\omega\hat{\varphi}_s = -2eZ_E I_c\hat{i}_s \quad (38)$$

$$|Z_E|^2(\omega) = |R_d|^2|\sqrt{G(\omega)} - 1|^2/4 \quad (39)$$

$$i\hbar\omega\hat{\varphi}_j = \frac{2eRI_c}{1+i\omega RC_J}\left(-\hat{i}_j + \hat{i}_n\right), \quad (40)$$

where i_n denotes the quantum noise from the shunt resistor; its spectral density reads $S_I(\omega) = 2\hbar\omega/(RI_c^2)$ in the dimensionless form. The spectrum of $\cos\varphi_s$ consists of a dc component and the even multiples of ω_s, whereas the spectrum of $\sin\varphi_s$ contains all odd harmonics of ω_s. We assume that Josephson frequency is large: $N = \omega_J/\omega_s \gg 1$. We write down explicitly the convolution in the first phase-to-current relationship:

$$\hat{i}_s = \frac{1}{4\pi}\int\left(\widehat{e^{i\varphi_s}}(s)\hat{\varphi}_j(\omega-\omega_J-s) + \widehat{e^{-i\varphi_s}}(s)\hat{\varphi}_j(\omega+\omega_J-s)\right)ds \quad (41)$$

$$\hat{\varphi}_j = \frac{2eRI_c}{i\hbar\omega(1+i\omega RC_J))}\left(-\hat{i}_j + \hat{i}_n\right), \quad (42)$$

where (after neglecting some terms containing $2\omega_J$)

$$\hat{i}_j(\omega-\omega_J-s) = \frac{i}{2}\widehat{e^{-i\varphi_s}}(\omega-s) \quad (43)$$

$$\hat{i}_j(\omega+\omega_J-s) = -\frac{i}{2}\widehat{e^{i\varphi_s}}(\omega-s) \quad (44)$$

$$\hat{\varphi}_j(\omega-\omega_J-s) = \frac{2eRI_c(\hat{i}_n(\omega-\omega_J-s) - \frac{i}{2}\widehat{e^{-i\varphi_s}}(\omega-s))}{i\hbar(\omega-\omega_J-s)(1+i(\omega-\omega_J-s)RC_J)} \quad (45)$$

$$\hat{\varphi}_j(\omega+\omega_J-s) = \frac{2eRI_c(\hat{i}_n(\omega+\omega_J-s) + \frac{i}{2}\widehat{e^{i\varphi_s}}(\omega-s))}{i\hbar(\omega+\omega_J-s)(1+i(\omega+\omega_J-s)RC_J)}. \quad (46)$$

Here $\omega - s$ takes the values $0, \pm\omega_s, \pm 2\omega_s, \pm 3\omega_s$, etc, all of which are small compared with ω_J. We approximate $\omega \pm \omega_J - s \approx \pm\omega_J$ in the denominators.

Let us consider downmixing and upmixing separately, using only the first pair of sidebands. Then $\hat{\varphi}_j$ has nonzero contributions around $\omega_J - \omega_s$, ω_J, $\omega_J + \omega_s$, and the corresponding negative frequencies. We expand the exponentials of φ_s using Bessel functions of

the first kind: $\exp(\pm i\varphi_s) \approx J_0(r) \pm i(2J_1(r)/r)\varphi_s$. φ_s is in the time domain here, while the Bessel terms are stochastic and will be time averaged later. Weak fluctuations in signal band are characterized by $r \approx 0$ and the exponential can be replaced by unity. In the limit of very strong fluctuations, additional terms with $J_2(r)$, $J_3(r)$, and so on may be required. As r is Rayleigh distributed, we obtain expectation values $\langle J_0(r)\rangle = \exp(-\delta_s^2/2)$ and $\langle 2J_1(r)/r\rangle = (1-\exp(-\delta_s^2))/\delta_s^2$ (see Eq. (30) and Ref. [1]). Upmixing is described by

$$\begin{aligned}\hat{\varphi}_j(\omega_J+\omega) &\approx \frac{2eRI_c[\hat{i}_n(\omega_J+\omega) + i\widehat{e^{i\varphi_s}}(\omega)/2]}{i\hbar\omega_J(1+ix)} \\ \hat{\varphi}_j(-\omega_J+\omega) &\approx \frac{2eRI_c[\hat{i}_n(-\omega_J+\omega) - i\widehat{e^{-i\varphi_s}}(\omega)/2]}{-i\hbar\omega_J(1-ix)}.\end{aligned} \tag{47}$$

Fourier transforming,

$$\widehat{e^{\pm i\varphi_s}}(\omega) = 2\pi J_0(r)\delta(\omega) \pm i(2J_1(r)/r)\hat{\varphi}_s(\omega). \tag{48}$$

The Josephson frequency is converted to dimensionless bias voltage v_b via $\hbar\omega_J = 2eV_b = 2eRI_cv_b$. We note that $x = \omega_J RC_J = \beta_c v_b$ where $\beta_c = 2eR^2I_cC_J/\hbar$. Downmixing is governed by

$$\hat{i}_s(\omega) = \frac{1}{4\pi}\int[(2\pi J_0\delta(s) + i\alpha\hat{\varphi}_s(s))\hat{\varphi}_j(\omega-\omega_J-s) + (2\pi J_0\delta(s) - i\alpha\hat{\varphi}_s(s))\hat{\varphi}_j(\omega+\omega_J-s)]ds \tag{49}$$

where α equals $2J_1(r)/r$. In order to make the analysis self-consistent, we plug in φ_j as a function of φ_s, see Eq. (47). After simplifying

$$\widehat{\varphi}_j(\omega_s-\omega_J)+\widehat{\varphi}_j(\omega_s+\omega_J) = \frac{1}{iv_b}\left(-\frac{\hat{i}_n(-\omega_J+\omega_s)}{1-ix} + \frac{\hat{i}_n(\omega_J+\omega_s)}{1+ix} - \frac{\alpha\hat{\varphi}_s(\omega_s)}{2}\left(\frac{1}{1+ix}-\frac{1}{1-ix}\right)\right), \tag{50}$$

we are left with

$$\hat{i}_s(\omega_s) = \frac{J_0}{2iv_b(1+x^2)}\left((1-ix)\hat{i}_n(\omega_J+\omega_s) - (1+ix)\hat{i}_n(-\omega_J+\omega_s)\right). \tag{51}$$

By definition, the squared modulus of the Fourier transform is directly proportional to the power spectral density. We are interested in one-sided ($\omega > 0$) power spectral densities which receive contributions from positive and negative frequencies:

$$S_I(\omega) \propto |\hat{i}_s(\omega)|^2 + |\hat{i}_s(-\omega)|^2. \tag{52}$$

The total noise power from the sidebands is estimated by $S_I(\omega_J-\omega_s)+S_I(\omega_J+\omega_s) \approx 2S_I(\omega_J)$.

$$S_I(\omega_s) = \frac{J_0^2}{4v_b^2(1+x^2)} \cdot 2S_I(\omega_J). \tag{53}$$

Next, the stochastic term is time averaged: $J_0^2 \to \langle J_0^2 \rangle$. We take its expectation value with respect to the Rayleigh distributed noise amplitude in Eq. (30):

$$\langle J_0^2 \rangle = \int_0^\infty J_0^2(r) \frac{r}{\delta_s^2} e^{-r^2/(2\delta_s^2)} dr. \tag{54}$$

$\langle J_0^2 \rangle$ will differ significantly from unity only if phase variance is large, $\delta_s^2 > 1$, which would be a consequence of high gain. Interestingly, in the limit of vanishing capacitance ($x = \omega_J RC_J \approx 0$), high bias ($v_b \approx I_b/I_c$) and low gain ($\langle J_0^2 \rangle \approx 1$) we arrive at the Koch-Clarke formula [4] for down-mixed noise

$$S_I(\omega) = \frac{I_c^2 S_I(\omega_J)}{2I_\mathrm{b}^2}. \tag{55}$$

We note that the DC current through the junction can be derived from the downmixing equation (49). It is essential that shunt capacitor C is not visible at Josephson frequency, otherwise the IV curve will change. Hence, we require $\omega_J RC \gg 1$ and study the limit $\omega_s \to 0$:

$$\begin{aligned} \hat{i}_s(0) &= \frac{1}{4\pi} \int \left[\widehat{e^{i\varphi_s}}(s) \left(\frac{2\pi J_0 \delta(s)}{2v_b(1-ix)} \right) + \widehat{e^{-i\varphi_s}}(s) \left(\frac{2\pi J_0 \delta(s)}{2v_b(1+ix)} \right) \right] ds \\ &= \frac{J_0}{4v_b} \left(\frac{\widehat{e^{i\varphi_s}}(0)}{1-ix} + \frac{\widehat{e^{-i\varphi_s}}(0)}{1+ix} \right) = \frac{J_0^2 \hat{1}}{2v_b(1+x^2)}. \end{aligned} \tag{56}$$

The DC current generator in parallel to the junction is $-\langle i_s \rangle = -\langle J_0 \rangle^2/(2v_b(1+x^2))$. As a consequence, the total bias current does not entirely flow through the shunt resistor. In the limit of small phase fluctuations, $\langle J_0^2 \rangle \approx 1$, the dynamic resistance of the junction at signal frequency will be

$$r_d = R_d/R = (d\langle i_s \rangle / dv_b)^{-1} = -\frac{2v_b^2(1+x^2)^2}{1+3x^2}. \tag{57}$$

We note that this result agrees with a previous study where the authors used perturbation theory to solve the IV curve for a resistively and capacitively shunted junction at high bias [6]. The result reads $v_b = i_b - [2i_b(1+\beta_c^2 i_b^2)]^{-1}$. After differentiation,

$$r_d = \frac{1}{\left(\frac{\partial v_b}{\partial i_b}\right)^{-1} - 1} = -\frac{2v_b^2(1+x^2)^2 + 1 + 3x^2}{1+3x^2} \tag{58}$$

where $v_b^2 \approx i_b^2$. The two expressions for r_d differ by a factor -1, which is negligible especially when $\beta_c > 0$. This is the first point where we observed discrepancy between the analytic model and the Langevin simulation. In the limit of large phase fluctuations, $\langle J_0^2 \rangle < 1$, the IV curve at DC should change according to analytic Eq. (56), but we did not notice any modification at variances up to $\delta_s^2 = 1.2$ in the simulation. We believe that the analytic model fails due to the inclusion of a single sideband pair only. The amplitudes of higher sidebands starting from $\omega_J \pm 2\omega_s$ are considerably large at high Josephson frequency as well as at large variance δ_s^2.

In the conversion of Eq. (53) to input noise temperature, we keep the $\langle J_0^2 \rangle$ modification even though it appears to be incomplete in the limit of large phase fluctuations.

$$k_B T_{\rm mix} = \frac{eI_c|R_d|}{2v_b} \left(\frac{G_m - 1}{G_m} \right) \frac{\langle J_0^2 \rangle}{1 + (\beta_c v_b)^2}. \tag{59}$$

The maximal gain is G_m. In the limit of high gain, $G_m \gg 1$, the term $(G_m - 1)/G_m \approx 1$ can be dropped out. At intermediate gain, on the other hand, we consider a cascade of similar amplifiers. Noise temperature from the Friis formula is

$$T_{\rm mix} \left(1 + \frac{1}{G_m} + \frac{1}{G_m^2} + \dots \right) \rightarrow \frac{T_{\rm mix}}{1 - 1/G_m} = \frac{G_m T_{\rm mix}}{G_m - 1}. \tag{60}$$

As a consequence, the gain dependence vanishes in a multistage cascade. Our dynamic resistance for high bias (Eq. (57), $v_b \geq 3$) is inserted into Eq. (59), and we obtain

$$\frac{k_B T_{\rm mix}}{\hbar \omega_s} = \frac{N \xi(\delta_s^2)}{2} \left(\frac{1 + \beta_c^2 v_b^2}{1 + 3\beta_c^2 v_b^2} \right) \tag{61}$$

which represents the number of added quanta at $N = \omega_J/\omega_s \gg 1$. The suppression of noise is included in the unknown function $0 < \xi(\delta_s^2) \leq 1$ which equals $\langle J_0^2 \rangle$ when noise is mixed down from the first pair of sidebands. It's obvious from Eq. (61) that low Josephson frequency and moderate junction capacitance improve the noise performance.

We have studied the breakdown of Eq. (61) at small N. The sideband pair will become asymmetric in phase and its spectral density. A correction term can be derived by starting from Eqs. (45) and (46) and retaining the antisymmetric $\omega_J - \omega_s$ and $\omega_J + \omega_s$ in the Josephson band:

$$\frac{N^2(1 + N^2 y^2)(1 + (N^2 + 3)y^2)}{(N^2 - 1)(1 + 2(N^2 + 1)y^2 + (N^2 - 1)^2 y^4)}, \tag{62}$$

where $y = \omega_s R C_J$. Eq. (61) must be multiplied by Eq. (62) which equals unity at high N. The correction term is significant at small N, and later we will show that the stan-

dard quantum limit, added noise of $\frac{1}{2}\hbar\omega_s$, cannot be reached in the limit of small phase fluctuations.

C. Bandwidth

The gain-bandwidth product of the SJA is $|\Gamma(\omega_s)|\Delta\omega_{-3\mathrm{dB}}$. We postulate that the gain function $G(\omega)-1$ has a peaked, Lorentzian form:

$$G(\omega)-1=\frac{G_m-1}{1+\left(\frac{2Q_s(\omega_s-\omega)}{\omega_s}\right)^2} \tag{63}$$

with the maximal gain of G_m. The full width at half maximum $\Delta\omega_{-3\mathrm{dB}}$, or FWHM, is denoted by ω_s/Q_s where Q_s is the quality factor at the signal frequency. The integral over the Lorentzian peak equals

$$\int_0^\infty (G(\omega)-1)df=\frac{1}{2\pi}\frac{\omega_s(G_m-1)}{Q_s}\frac{\pi}{2}=\frac{\omega_s(G_m-1)}{4Q_s}. \tag{64}$$

The quality factor arises from the resonator $L, C+C_J$ which is loaded with the real part of Z_E.

$$Q_s=\mathbb{R}\{Z_E\}\sqrt{\frac{C+C_J}{L}}\approx\omega_s|Z_E(\omega_s)|(C+C_J)=\frac{1}{2}|R_d|(\sqrt{G_m}-1)\omega_s(C+C_J). \tag{65}$$

The minimal shunt capacitance is set by the shunt resistance and the Josephson frequency: $R=\alpha_C\cdot(\omega_J C)^{-1}$, $\alpha_C\gg 1$. Thus, we may write

$$C+C_J=\frac{\alpha_C}{\omega_J R}+C_J=\frac{\hbar(\alpha_C+x)}{2eR^2I_c v_b}. \tag{66}$$

By using the Q-factor in Eq. (65) and the representation of the capacitance, Eq. (66), we obtain

$$|\Gamma(\omega_s)|\Delta\omega_{-3\mathrm{dB}}=\frac{4eRI_c}{\hbar}\left(\frac{\sqrt{G_m}}{\sqrt{G_m}-1}\right)\frac{v_b}{|r_d|(\alpha_C+x)}\approx\frac{N\omega_s\sqrt{G_m}}{\sqrt{G_m}-1}\cdot\frac{1+3x^2}{v_b^2(1+x^2)^2(\alpha_C+x)}. \tag{67}$$

Eq. (67) indicates that high bandwidth is reached when the critical current is large and the dynamic resistance $|r_d|$ is small; most effectively this is achieved by tuning down the dimensionless bias voltage.

D. Stability

In the stable operating mode of the amplifier, we do not allow zero crossings for the Josephson voltage fluctuations around the steady-state bias v_b. Instability of the amplifier is characterized by a spontaneous pattern of the Josephson voltage v at the signal frequency as well as extra harmonic content in the spectrum. We know that the origin of the fluctuations is either (i) noise from the amplifier input, (ii) down-mixed noise, or (iii) direct noise from the shunt resistor. We derive the variance of the dimensionless voltage noise for the first two cases, $\sigma_{\rm in}^2$ and $\sigma_{\rm mix}^2$, respectively. The direct noise, discussed in Ch. II A, is small and it is neglected. Since these variances are uncorrelated and the standard deviation of the junction voltage becomes $\sigma = \sqrt{\sigma_{\rm in}^2 + \sigma_{\rm mix}^2}$. For stability reasons, there needs to be an operational margin for voltage fluctuations, which we approximate as $3\sigma < v_{\rm b}$. We will later observe that this requirement leads to an upper bound for the available gain, since σ increases with gain.

1. Input noise

The voltage transfer function from the input to the junction is given by

$$\left|\frac{v}{v_{\rm sg}}\right|^2 = \frac{|R_d|(G-1)}{4Z_0}. \tag{68}$$

The power spectral densities, S_g at the input and S_v at the junction, are linked in a similar fashion:

$$S_v = S_g \cdot \frac{|R_d|(G-1)}{4Z_0}. \tag{69}$$

The quantum noise at the input has the form

$$S_g = \frac{2Z_0\hbar\omega_s \coth(\hbar\omega_s/(2k_BT_{\rm input}))}{R^2I_c^2}. \tag{70}$$

The variance of the junction voltage, $\sigma_{\rm in}^2$, equals the power given by the integral of S_v over frequency, see Eq. (69).

$$\int S_v df = \sigma_{\rm in}^2 = \frac{\hbar\omega_s|R_d|}{2R^2I_c^2} \coth\left(\frac{\hbar\omega_s}{2k_BT_{\rm input}}\right) \int (G(\omega)-1)df. \tag{71}$$

The gain integral is evaluated in Eq. (64):

$$\int (G-1)df = \frac{\sqrt{G_m}+1}{2|R_d|(C+C_J)}. \tag{72}$$

Finally, by combining the equations above,

$$\sigma_{\rm in}^2 = \frac{\omega_s e v_b(\sqrt{G_m}+1)}{2I_c(\alpha_C+\beta_c v_b)} \coth\left(\frac{\hbar\omega_s}{2k_B T_{\rm input}}\right). \tag{73}$$

The central conclusion here is that the critical current I_c cannot be made small.

2. *Down-mixed noise*

We derive the phase noise variance δ_s^2 due to downmixing (cf. Eq. (51)) using frequency domain integrals. We observe from Eq. (38) that $\hbar^2\omega^2 S_\varphi = (2eZ_E I_c)^2 S_I(\omega)$ which can be integrated with respect to frequency using Eq. (53) for $S_I(\omega)$:

$$\frac{\hbar\omega^2 S_\varphi}{2} = \left(\frac{eI_c}{2v_b}\right)^2 \frac{\langle J_0^2\rangle \cdot 4Z_E^2}{1+x^2} S_I(\omega_J), \tag{74}$$

$$\frac{\hbar^2\omega_s^2}{2}\int_0^\infty S_\varphi(\omega)df = \left(\frac{eI_c|R_d|}{2v_b}\right)^2 \frac{\langle J_0^2\rangle}{1+x^2}\int_0^\infty (\sqrt{G(\omega)}-1)^2 S_I(\omega_J)df \tag{75}$$

In Eq. (75) $(\sqrt{G}-1)^2$ converges to zero more rapidly than a Lorentzian:

$$\int_0^\infty (\sqrt{G}-1)^2 df = \int_0^\infty \left[(G-1)+2(1-\sqrt{(G-1)+1})\right] df < \int_0^\infty (G-1)df. \tag{76}$$

We define a correction factor κ to write the result of the above integral in terms of the result of Eq. (64):

$$\int_0^\infty (\sqrt{G(\omega)}-1)^2 df = \frac{\kappa\omega_s(G_m-1)}{4Q_s}. \tag{77}$$

The correction factor κ, displayed in Fig. 2, approaches 1 at large gain, but at small gain $\kappa << 1$. Thus, we may separate out the ratio of the variance δ_s^2 to $\langle J_0^2\rangle$:

$$\frac{\delta_s^2}{\langle J_0^2\rangle} = \frac{\kappa e^3 I_c|R_d|^2(G_m-1)}{2Q_s\hbar^2 v_b(1+x^2)\omega_s} = \frac{4\kappa e^4 R^3 I_c^2 v_{\rm b}^2(\sqrt{G_m}+1)(1+x^2)}{\hbar^3\omega_s^2(\alpha_C+x)(1+3x^2)}. \tag{78}$$

The variance is related to the voltage fluctuations via $\sigma^2 = \hbar^2\omega_s^2\delta_s^2/(2eRI_c)^2$. Considering the limit $\langle J_0^2\rangle = 1$,

$$\sigma_{\rm mix}^2 = \frac{\kappa e|r_d|(\sqrt{G_m}+1)}{4I_c R v_b(C+C_J)(1+\beta_c^2 v_b^2)} = \frac{\kappa e^2 R|r_d|(\sqrt{G_m}+1)}{2\hbar(1+\beta_c^2 v_b^2)(\alpha_C+\beta_c v_b)}. \tag{79}$$

Most importantly, $\sigma_{\rm mix}^2$ grows linearly with R, which has to be taken into account in the amplifier design.

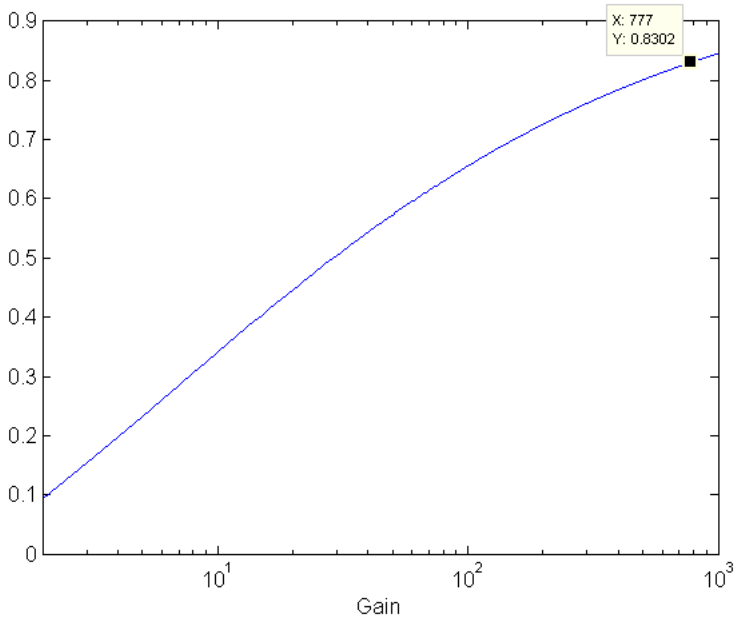

FIG. 2. Correction factor κ employed in expressing the integral Eq. (76) in terms of the result of Eq. (64).

III. PRACTICAL CONSIDERATIONS IN THE SJA DESIGN

The constraints that limit the available range of device parameters are listed in Table I. We extract some crucial relationships between R, I_c and C_J from the chapters above:

$$2eRI_c v_b = \hbar\omega_J = N\hbar\omega_s \tag{80}$$

$$N\omega_s RC_J = \beta_c v_b = x \tag{81}$$

$$|\Gamma(\omega_s)|\Delta\omega_{-3\mathrm{dB}} \propto \frac{N(1+3x^2)}{v_b^2(1+x^2)^2} \tag{82}$$

$$\sigma^2_{\mathrm{mix}} \propto Rv_b^2(\sqrt{G_m}+1) \tag{83}$$

$$\sigma^2_{\mathrm{in}} \propto \frac{v_b(\sqrt{G_m}+1)}{I_c} \tag{84}$$

A. Limit of small fluctuations

The optimization in the case of small fluctuations $\delta_s^2 \ll 1$ begins with studying the down-mixed noise (Eq. (61) with $\xi = 1$). At low bias, the Josephson frequency is relatively small: N has to be a fraction, e.g. 2.5 or 3.5, because sidebands of the Josephson frequency (and its

TABLE I. SJA boundary conditions; Shunt $R-L-C$, Josephson frequency ω_J, junction capacitance C_J, plasma frequency ω_p, voltage bias v_b, critical current I_c, $\beta_c = 2eR^2 I_c C_J/\hbar$.

Requirement	Solution
Shunt C not visible at ω_J	$\alpha_C = \omega_J RC = \beta_c v_b C/C_J > 1$
$\omega_p < \omega_J$	$\sqrt{\beta_c} v_b > 1$
$\omega_J > \omega_s$	$2eRI_c v_b > \hbar\omega_s$
Noise at ω_J is quantum	$2eRI_c v_b \gg k_B T_\mathrm{shunt}$
$\hbar\omega_J$ is smaller than gap	$\hbar\omega_J < \Delta$
Stability	I_c is large enough, R is small enough
High bias	$v_b \geq 3$
Minimal direct noise	$\omega_s \approx 1/\sqrt{LC}$

harmonics) must not coincide with the signal frequency. Eq. (67) reveals that the bandwidth of the amplifier will suffer both from a small N and from a high $\beta_c v_b$ ($\beta_c = 2eR^2 I_c C_J/\hbar$). Therefore, the noise optimization at $\delta_s^2 \ll 1$ is in conflict with a high bandwidth. The lower bound of v_b is found by (i) considering stability, i.e., forbidding zero crossings for the voltage fluctuations around v_b, (ii) remembering that high Josephson frequency (in practise, high v_b) was assumed in the calculations of Ch. II. By fixing N, the bias gives the product RI_c from Eq. (80). Stability can be improved by selecting a low R and a high I_c, because both σ_in^2 and σ_mix^2 will be decreased. Finally, fixing β_c gives x and the product RC_J. The disadvantages of a high RC_J will be discussed later. Guidelines for parameter selection are listed in Table II

B. Noise compression limit

The ultimate limit of noise compression, i.e., the exact form of $\xi(\delta_s^2)$, is unknown to us. It remains to be studied whether the standard quantum limit of added noise can be reached by means of compression. The non-linearities of the SJA will begin to limit the gain and alter the operation point when the variance of phase fluctuations grows beyond $\delta_s^2 = 1$. Here we analyze the simplest compression model $\xi(\delta_s^2) = \langle J_0^2 \rangle$, see Eq. (61). The ratio $\delta_s^2/\langle J_0^2 \rangle$ grows linearly with $(\sqrt{G_m} + 1)$ as shown in Eq. (78). The procedure of estimating noise

TABLE II. SJA parameters at low ω_J and δ_s^2. GBP is the gain-bandwidth product, σ^2 is the dimensionless variance of the Josephson voltage noise, and $\alpha_C = \omega_J RC$.

Parameter	Advantages	Disadvantages
Low R	Down-mixed noise stability σ^2_{mix}	Poor impedance matching
High I_c	Input noise stability σ^2_{in}	R becomes lower
Low N	Low down-mixed noise	Poor impedance mathing, low GBP, shunt must be at low temperature
High β_c	Low down-mixed noise, $\omega_p \ll \omega_J$	Poor impedance mathing, low GBP
High α_C	Stability, IV curve is accurate	Low GBP, direct noise grows rapidly when moving away from the shunt eigenfrequency

compression is numerical: there is a one-to-one correspondence between variance δ_s^2 and the ratio $\delta_s^2/\langle J_0^2\rangle$. The latter is exactly known and we can read it from a graphical plot in Fig. 3, where we also depict δ_s^2 and $\langle J_0^2\rangle$ separately. In the analytical modeling, we assume that the fluctuations of φ_s conform to a Rayleigh distributed amplitude (see Eq. (30)), although in the numerics there are observable deviations from this assumption. The compression factor is plotted as a function of gain in the lowest frame of Fig. 3. This graph defines the modification $0 < \langle J_0^2\rangle \leq 1$ of the input noise temperature obtained for the investigated amplifier using linear models.

IV. RESULTS

A. Reproduction of the experimental findings in the noise compression regime

The bandwidth of the numerical simulation was 1 THz, and the input noise at $T_{\mathrm{in}} = 70$ mK was bandpass filtered between 2.5 GHz and 3.5 GHz. The device parameters in the simulation are given in Table I of the main paper. The temperature of the shunt was set to $T_{\mathrm{shunt}} = 400$ mK,

The dynamic resistance of the junction was $-1370\ \Omega$ in the simulation and $-1350\ \Omega$ analytically. A 28.9 dB power gain was observed at high L_2 (measured gain was 28.3 ± 0.2 dB). The gain-bandwidth-product was 42 MHz, and the added noise was 270 ± 30 mK (40

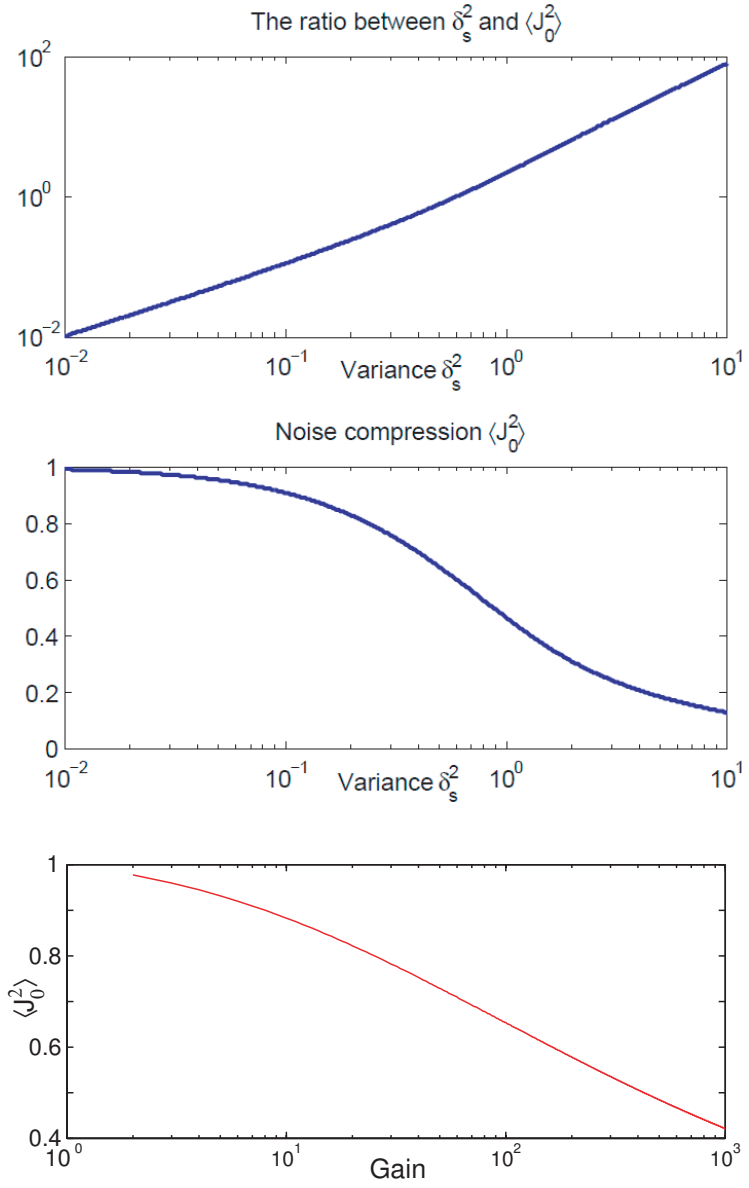

FIG. 3. Top frame: the ratio $\delta_s^2/\langle J_0^2 \rangle$ as a function of phase noise variance δ_s^2 in the signal band. Middle frame: noise compression as a function of the variance δ_s^2. Lowest frame: the suppression factor $\langle J_0^2 \rangle$ vs. gain for the parameters used in the experiments (this suppression factor was employed in Fig. 5 in the main paper).

MHz and 220 ± 70 mK in the experiment, respectively). Altogether, the simulation was in good agreement with the experiment.

B. Quantum limited amplifier without noise compression

We minimized the down-mixed noise at low bias ($v_\mathrm{b} \geq 3$) using Eqs. (61) and (62). In the best configurations, 0.9 noise quanta per unit band are added by the SJA. The optimum corresponds to $v_\mathrm{b} = 3$, $\beta_c = 0.3 - 0.5$ and $N = 2.1 - 2.6$. The device parameters of the best simulated amplifier are listed in Table III. The shunt eigenfrequency was 3.0 GHz and the shunt temperature was set to 100 mK. The gain reached 14.5 ± 0.2 dB and the output

TABLE III. The best simulated SJA. For the parameter definitions, see Ch. I of this Supplementary material. $\alpha_C = \omega_J RC$.

Parameter	Value	Parameter	Value
Z_0	2.5 Ω	I_c	1 μA
R	5 Ω	C_J	4.6 pF
C	45 pF	$\omega_\mathrm{p}/(2\pi)$	4.1 GHz
L	63 pH	β_c	0.35
C_2	33 pF	I_b	3 μA
L_2	0.69 nH	$\omega_\mathrm{J}/(2\pi)$	7.0 GHz
ω_s	3.0 GHz	α_C	10

noise power was equivalent to 6.3 ± 0.3 K. Our numerical simulation yielded 0.9 ± 0.2 quanta for the added noise, in excellent agreement with the analytic model. We also simulated six other amplifiers at the bias $v_\mathrm{b} = 3$. It was found that high RC_J may be responsible for the breakdown of the down-mixed noise model. The high RC_J modifies the phase differences induced by upmixing and downmixing processes. Several quanta of noise were added in some simulations at $\beta_c = 0.35 - 0.90$, even though the analytic expectation was about 1 quantum. At $\beta_c = 0.1$ the noise temperature was also very high, and we believe that this resulted from high plasma frequency $\omega_p > \omega_J$. Results consistent with our analytical model are plotted in Fig. 4.

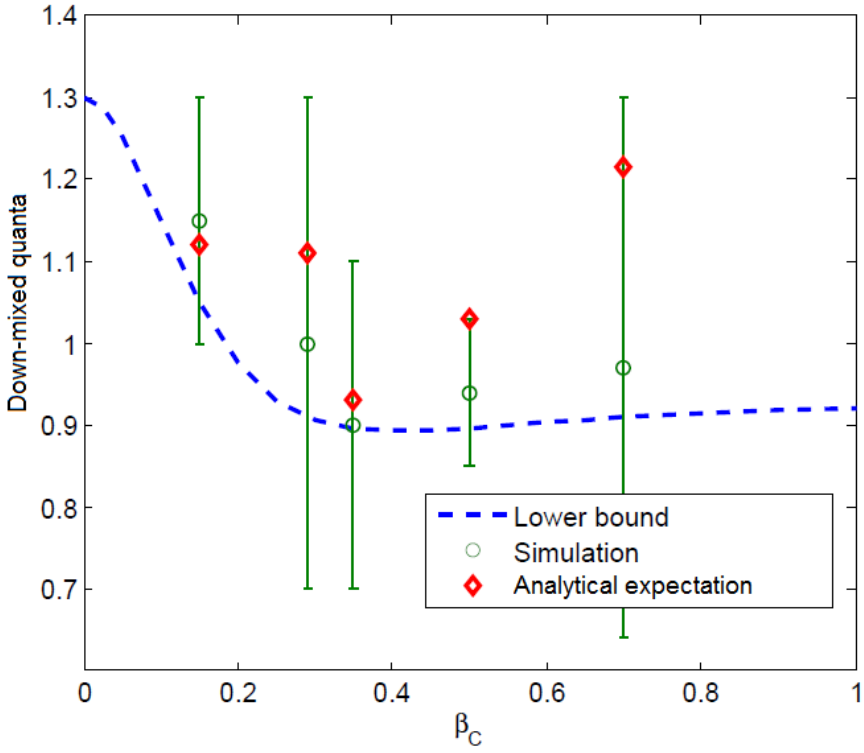

FIG. 4. Analytic model, Eqs. (61) and (62), yields a lower bound for added noise as a function of β_c. Several SJAs with varying parameters were simulated at $v_\mathrm{b} = 3$. Gain was in the range $G_m = 11.2 - 24.5$ dB and $N = \omega_J/\omega_s = 2.3 - 5.6$. Our analytic model predicts accurately the down-mixed noise contribution provided that $\omega_J > \omega_p$ and RC_J is small.

[1] M. Abramowitz and I. A. Stegun. *Handbook of Mathematical Functions with Formulas, Graphs, and Mathematical Tables*, U. S. Department of Commerce, 1972, Chap. 11.

[2] K. K. Likharev and V. K. Semenov. Fluctuation Spectrum in Superconducting Point Junctions, *JETP Lett.* **15**, 442 (1972).

[3] K. K. Likharev. *Dynamics of Josephson Junctions and Circuits*, Gordon and Breach, New York (1986).

[4] R. H. Koch, D. J. van Harlingen, and J. Clarke. Quantum-Noise Theory for the Resistively Shunted Josephson Junction, *Phys. Rev. Lett.* **45**, 2132 (1980).

[5] Y. Levinson. Quantum noise in a current-biased Josephson junction, *Phys. Rev. B* **67**, 184504 (2003).

[6] F. T. Brandt, J. Frenkel, and J. C. Taylor. Noise in resistively shunted Josephson junctions, *Phys. Rev. B* **82**, 014515 (2010).

[7] S. Haykin. *An Introduction to Analog and Digital Communications*, Wiley, New York, 1989.

[8] G. Arfken. *Mathematical Methods for Physicists*, Academic Press, New York, 1970, p. 482.